RSC Advances

ROYAL SOCIETY OF CHEMISTRY

www.rsc.org/advances

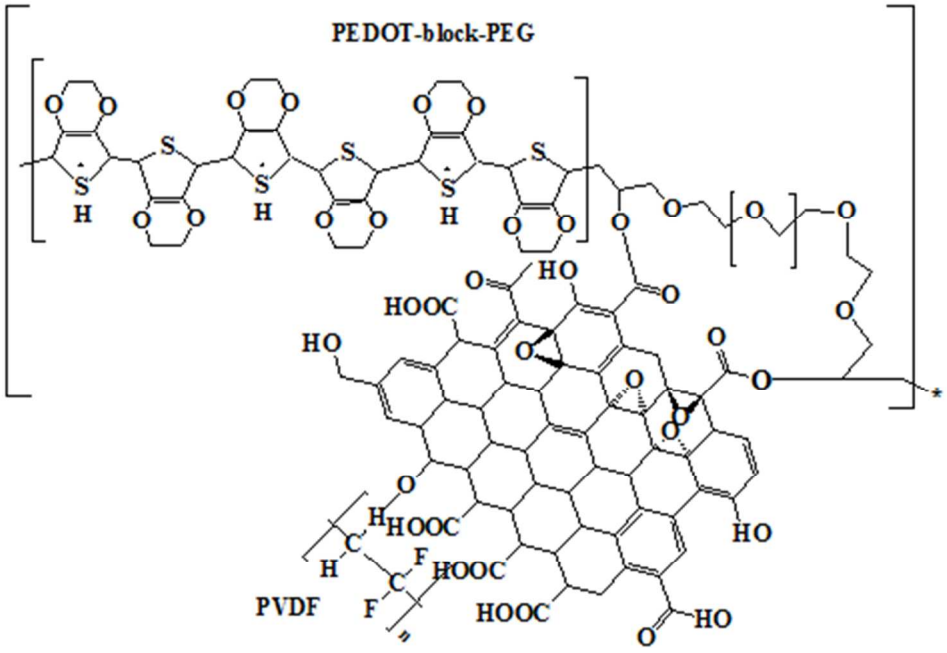

Novel Nanocomposites of Graphene Oxide Reinforced Poly (3, 4-ethylenedioxythiophene) - block-Poly (ethylene glycol) and Polyvinylidene fluoride for Embedded Capacitor Applications

Kalim Deshmukh, Girish M. Joshi

Polymer Nanocomposite Laboratory, Material Physics Division,
School of Advanced Sciences, VIT University, Vellore - 632014, TN, India

Corresponding author: Dr. Girish M. Joshi
Email:varadgm@gmail.com

Abstract

The fabrication and characterization of nanocomposites consisting of graphene oxide (GO) reinforced poly (3, 4 - ethylenedioxythiophene) – block - poly (ethylene glycol) (PEDOT-block-PEG)/polyvinylidenefluoride (PVDF) were investigated. The characterizations of nanocomposites were carried out using UV-vis spectroscopy, X-ray diffraction (XRD), Differential Scanning Calorimetry (DSC), Thermogravimetric analysis (TGA), Fourier transforms infrared (FTIR) and FT-Raman spectroscopy. Dielectric properties were investigated using an impedance analyzer as a function of frequency (50 Hz to 35 MHz) and temperature in the range (40-150^{o}C). Atomic force microscopy (AFM) was employed to study the surface morphology of nanocomposites. Atomic force microscopy reveals that the surface roughness increases as a function of GO loading. The presence of high surface area GO within the polymer matrix resulted in substantially improved thermal stability. Better dispersion resulted in an increase in the dielectric constant from 58.684 for 0.5 wt% to 266.091 for 3 wt% GO loading and dielectric loss from 1.758 for 0.5 wt % GO to 17.694 for 3 wt % GO. High values of dielectric constant are obtained with comparatively low dielectric loss. Hence, polymer nanocomposites with high dielectric constant and low dielectric loss have the potential to be used in electronic and electric industry.

Keywords: Graphene oxide; PEDOT- Block- PEG; PVDF; Dielectric Constant

Introduction

Graphene is a monolayer of carbon atoms consisting of sp^2 hybridized carbon layer arranged in two dimensional honeycomb lattices.[1] The conjugated π- electron along with the two dimensional network leads to unique and extraordinary properties which includes, high electron mobility at room temperature[2], exceptional thermal conductivity[3], and superior mechanical properties.[4] The superior properties of graphene make it suitable for use as inorganic filler to improve the electrical, thermal and mechanical properties of polymer nanocomposites.[5] Graphene has been used as a promising material for the potential applications which includes detection of single gas molecule[6], energy storage devices such as super or ultracapacitors[7], transparent conducting electrodes[8], fabrication of transistors[9] and lithium ion batteries[10]. Many efforts have been put towards the synthesis of pristine graphene using different techniques such as chemical vapor deposition (CVD) [11], epitaxial growth[12], and mechanical cleavage.[2] Mechanical exfoliation of highly ordered pyrolitic graphite (HOPG) is a common method to produce large quantity of graphene sheets having different microscopic dimensions.

Another important and useful member of graphene family is graphene oxide (GO). Conventionally, GO serves as a precursor material for the synthesis of graphene. GO consist of two dimensional network of sp^2 and sp^3 bonded carbon atoms arranged in a honeycomb structure.[13] The formation of sp^3 domains in GO is due to the oxidation reaction which results in the decoration of highly reactive oxygenated functional groups such as carbonyl, carboxyl and epoxy. [14] These highly reactive functional groups promotes good dispersibility of GO in water and allows it to be easily exfoliated in polar solvents. The maximum dispersibility of GO in solution is important for processing and further functionalization. It was reported that greater the polarity of the surface the greater the dispersibility.[15] For large scale applications such as for supercapacitors, reduction of GO is the most feasible and desirable choice to produce large quantity of graphene. Furthermore, GO itself has several applications in various fields such as memory devices, supercapacitors, optoelectronics, photo catalysis, ion conductor, drug delivery and as a reinforcing filler for the fabrication of GO based polymer nanocomposites.[14, 16-20] This has drawn the attention of many researchers all over the world to explore the fascinating properties of GO.

Because of their large number of unique features and easy preparation, conducting polymers (CPs) have been of tremendous importance in the field of material science. They are also known as synthetic metals. Conducting polymers have broad perspective in a wide range of applications such as thin film transistors[21], electromagnetic shielding[22], biosensors[23], actuators [24] and supercapacitors.[25] Various π-conjugated semiconducting polymers such as polypyrrole (PPy), polyvinylcarbazole (PVK), polyaniline (PANI), polyparaphenlyenevinylene (PPV), polyacetylene (PA), polythiophene and their derivatives have been studied extensively during the last few years. These are a class of polymers containing a large resonating structure with many sp^2carbon atoms. Conducting polymers based on polythiophene are widely used in manufacturing of flexible organic or hybrid electronic devices such as displays, transistors, photovoltaic cells, sensors, electroluminescent lamps etc.[26]. Poly (3, 4-ethylenedioxythiophene) (PEDOT) has attracted much attention in the field of conducting polymer because of its unique properties such as high conductivity and structural stability. When it is doped with polystyrenesulfonate (PSS), reasonable optical transparency can be obtained when used as a film.[27]

Nanocomposites of intrinsically conducting polymers has been studied extensively because these nanocomposites can combine the effect of each component and results in the improvement of the properties due to possible synergistic effect. Thus with this interest, herein we report, the development and characterization of GO reinforced PEDOT-block-PEG/PVDF based novel nanocomposites. The reason for choosing PEDOT-block-PEG and PVDF Polymer in the present study is that PEDOT-block-PEG has good optical transparency, good processability and environmental stability. It is anticorrosive in nature which is suitable for naval and marine applications. The block copolymer structure of PEDOT-block-PEG renders high dispersibility in organic solvents. On the other hand, PVDF has good dielectric properties. It is a crystalline polymer which has good film forming ability. PVDF has been used for number of applications including polymer sensors, transducers, actuators and hydrophone applications. To the best of our knowledge, there are no reports on GO incorporated PEDOT-block-PEG/PVDF nanocomposites. Herein, for the first time we report the fabrication and characterization of PEDOT-block-PEG/PVDF/GO nanocomposite films by solution blending. The effect of GO loading on thermal stability, structural, morphological and dielectric properties of GO reinforced

PEDOT-block-PEG/PVDF nanocomposites was demonstrated and related mechanisms were discussed.

Experimental

Materials

Graphite was supplied by Carbotech Engineers PVT, Ltd, Jaipur, India. GO was synthesized using natural graphite according to the modified Hummers method. [28, 29] Poly (3, 4 - ethylenedioxythiophene) – block - poly (ethylene glycol) (PEDOT- block- PEG) of molecular weight 1300-1600 g/m, resistance 1-10 MΩ/sq (surface resistance of film), bulk conductivity 01-0.5 S/cm and density 1.127 g/ml at 25^{o}C was purchased from Sigma Aldrich, India. Polyvinylidenefluoride (PVDF) powder was obtained from Pragati Plastics PVT, Ltd, India. Dimethylformamide (DMF) of research grade was purchased from Sisco Research Laboratories, PVT, Ltd., India.

Preparations of PEDOT- block- PEG /PVDF/ GO nanocomposite films

PEDOT-block-PEG/PVDF/GO nanocomposites films were prepared using solution casting. First, GO powder was dispersed in DMF and sonicated for 30 min at room temperature. PVDF was used as a polymer binder and was separately dissolved in DMF at 60^{o}C. A known quantity of PEDOT-block-PEG solution was added to PVDF/GO dispersion. The mixture was further sonicated for 30 min. The resulting homogeneous dispersion was cast on to a glass Petri dish and kept in an oven at 60^{o}C (for 8 hr) for slow evaporation of the solvent. Pristine nanocomposites film consisting of PEDOT-block-PEG/PVDF/GO were peeled off from the glass plate and used for further study. The % loading of GO in PEDOT-block-PEG/PVDF/GO nanocomposites was controlled from 0.5 wt% to 3 wt%. A schematic representation of the bonding interaction between PEDOT-block-PEG, PVDF and GO is shown in Figure 1. The protocol for synthesis is depicted in Figure 2.

Characterization of PEDOT-block-PEG/PVDF/ GO nanocomposite film

FTIR spectroscopy of PEDOT-block-PEG/PVDF/GO nanocomposites film was carried out with Fourier Transform Infrared Spectrophotometer (Shimazdu, IRAffinity-1, Japan) in the wave number range 400 – 3500 cm^{-1}. The spectra were taken in a transmittance mode.

Raman spectroscopy PEDOT-block-PEG/PVDF/GO nanocomposites film was carried out on Raman Scattering Spectrometer (LABRAM HR 800) by using a 633 nm laser at room temperature in backscattering mode.

UV–vis absorption spectroscopy of PEDOT-block-PEG/PVDF/GO nanocomposites was obtained with a Shimazdu UV-2401PC, UV–vis spectrophotometer in the range of 200–600 nm.

X-ray diffraction of PEDOT-block-PEG/PVDF/GO nanocomposites film was recorded using Cu Kα radiation of wavelength λ = 1.54060 Å with a graphite monochromator produced by Bruker AXS D8 focus advance X-ray diffraction meter (Rigaku, Japan, Tokyo) with 'Ni-filtered'. The scans were taken in the 2θ range from 4-80^o with a scanning speed and step size of 1^o/mm and 0.01^o respectively.

DSC thermograms of PEDOT-block-PEG/PVDF/GO nanocomposites film was evaluated by using DSC 8000 advanced double furnace differential scanning calorimeter (Perkin Elmer) at a heating rate of 10^{o}C/min. under N_2 atmosphere in the temperature range 50-300^{o}C.

Thermal stability of PEDOT-block-PEG/PVDF/GO nanocomposites film was evaluated by a TA Q 500 thermo gravimetric analyzer (TGA) operated under N_2 as a purge gas. Samples were heated up to 600^{o}C at a rate of 20^{o}C/min.

The morphology of PEDOT-block-PEG/PVDF/GO nanocomposites film was determined by typical tapping mode atomic force microscopy (NanoSurf Easy Scan2, Switzerland), operating in air. For AFM study samples were prepared by sticking a small piece of nanocomposites film on a glass slide.

The dielectric properties were measured using a Newton's 4th Impedance Analyzer (Newtons 4th UK) as a function of frequency in the range of 50 Hz to 35 MHz and temperature in

the range of 40-150^{o}C with an accuracy of about $\pm$ 0.1^{o}C. For better electrode contact, the nanocomposites films were silver coated from both sides.

Results and Discussions

FTIR Spectroscopy

The FTIR spectra were recorded to explore the reactive functional groups of GO and to study the interaction between GO, PEDOT-block-PEG and PVDF. The FTIR spectra of GO, PEDOT-block-PEG, PVDF and PEDOT-block-PEG/PVDF/GO nanocomposite films are shown in Figure 3 and Figure 4 respectively and the peak assignments are given in Table 1. The FTIR spectrum of GO shows peaks at 3419 cm^{-1} which correspond to O-H stretching vibration, a peak at 1720 cm^{-1} which corresponds to C=O stretching of carbonyl/carboxyl group. The peak at 1643 cm^{-1} is also observed which corresponds to C=C of unoxidized sp^2 group and the peak at 1404 cm^{-1} can be attributed to C-O stretching vibrations of carboxylic group. [20, 29] The peak at 1124 cm^{-1} can be attributed to C-O stretching vibration of alkoxy group. Thus, from the FTIR spectrum of GO it is evident that different functional groups such as carbonyl, hydroxyl and epoxy groups are present in GO. The FTIR spectrum of PEDOT-block-PEG shows several characteristic peaks. The peak at 979 cm^{-1}, 835 cm^{-1} and 623 cm^{-1} can be attributed to C-S bonds in PEDOT-block-PEG polymer chains.[30, 31] The peaks at 1571 cm^{-1} and 1400 cm^{-1} can be attributed to C=C stretching vibrations.[30] The peak at 1083 cm^{-1} appears due to C-H in plane bending vibration. Also the peak at 2933 cm^{-1} could be assigned to aromatic C-H stretching vibrations of PEDOT-block-PEG. The FTIR spectrum of PVDF shows two distinct absorption bands at 2974 cm^{-1} and 3012 cm^{-1} which can be attributed to symmetric and asymmetric stretching vibrations of CH_2 group.[32] Also peaks at 1064 cm^{-1}, 842 cm^{-1} and 588 cm^{-1} can be attributed to CF_2 stretching, CH_2 rocking and CF_2 bending vibrations respectively.[33, 34] The FTIR spectra of PEDOT-block-PEG/PVDF/GO nanocomposite film show various FTIR peaks which are common between the FTIR of individual components, indicating that the significant interaction has occurred between them. Thus, from the FTIR spectra, we can suggest successful formation of PEDOT-block-PEG/PVDF/GO nanocomposite.

Raman Spectroscopy:

Raman scattering is strongly sensitive to the electronic structure of samples and its results are often taken as an evidence for the chemical functionalization of graphite materials. The main features of graphene based materials which can be studied using Raman spectroscopy are G and 2D band. The G band originates from sp^2 bonded carbon atom, the 2D band originates from a two phonon double resonance Raman process and the D band is the result of a single phonon lattice vibrational process.[35] Figure 5 shows the Raman spectra of pristine graphite, GO and PEDOT-block-PEG/PVDF/GO nanocomposites. The Raman spectrum of pristine graphite shows an intense G band at 1582.50 cm^{-1}, 2 D band at 2702.18 cm^{-1} and weak D band at 1349.10 cm^{-1}. The Raman spectrum of GO shows a prominent D band at 1355.06 cm^{-1} indicating that the sp^2 domains are decreased due to extensive oxidation.[36] Also the G band of GO is broadened and shifted to 1606.36 cm^{-1}. This indicates that the isolated double bonds of GO are resonated slightly at higher frequencies as compare to pristine graphite. It is understood that the harsh chemical oxidation process will results in predominant structural changes in the graphite lattice due to formation of different types of oxygenated functional groups at the basal plane and at the edges. For nanocomposites with 1 wt % GO loading, the D and G bands are shifted to 1605.56 cm^{-1} and 1795.22 cm^{-1} respectively. At 2.5 wt % GO loading, the D and G bands were shifted to 1439.36 cm^{-1} and 1510.13 cm^{-1} respectively which can be attributed to restoration of sp^2 hybridized carbon.

UV-visible Spectroscopy

The UV absorption spectroscopy is used for the investigation of optical properties of polymeric materials. The absorption of light energy by polymeric materials in UV and visible region involves promotion of electrons in σ, π and n- orbitals from ground state to higher energy states.[37] The UV-vis spectra for PEDOT-block-PEG/PVDF/GO nanocomposite in DMF are shown in Figure 6. The inset image is the UV-vis spectrum of GO, which exhibits a maximum absorption peak at about 230 nm, which is corresponding to $\pi - \pi^*$ transitions of aromatic C-C bonds. For PEDOT-block-PEG/PVDF/GO nanocomposites, the absorption peak was red shifted to 267 nm which indicates that substantial amount of interaction has taken place between PEDOT-block-PEG, PVDF and GO. This phenomenon of red shift from 230 nm to 267 nm has been used to monitor the restoration of the conjugated π structure. The $\pi - \pi$ interaction between

positively charged PEDOT-block-PEG and negatively charged GO has helped in the formation of PEDOT-block-PEG/PVDF/GO nanocomposites.

XRD analysis

The XRD pattern of PEDOT-block-PEG/PVDF/GO nanocomposite films is shown in Figure 7. The XRD pattern of GO shows only a single characteristic (002) diffraction peak at 2θ = 10.25°, which corresponds to the interlayer distance d_{002} = 8.418 Å.[38] This indicates that the natural graphite is oxidized into GO which disrupts the ordering of layers and introduces functional groups to the graphite sheets. The peak represents second order reflections arising from the interlayer spacing, indicating that the interlayer distance obviously increases due to intercalation of oxide functional groups compared to the pristine graphite.[39] A broad diffraction peak was observed in the range 2θ = 18.984° to 2θ = 19.214° for all nanocomposites films with different wt% of GO loading. These diffraction peaks (110) belong to β crystalline phases of PVDF. The d- spacing values decreased from 4.671 to 4.633 Å. The decrease in d-spacing values can be due to induction of stress which results from the intermolecular interaction of PEDOT-block-PEG, PVDF and reinforced GO. This implies that the homogeneous dispersion of GO in polymer matrix was achieved which results in the successful preparation of PEDOT-block-PEG/PVDF/GO nanocomposite.

Thermal Analysis

The thermal analysis of PEDOT-block-PEG/PVDF/GO nanocomposites was studied using DSC and TGA. The DSC results are depicted in Figure 8 and Figure 9 where melting and crystallization temperatures were shown for nanocomposites with different wt% of GO loading. The melting temperature has increased from 142.63°C for 0.5 wt % GO loading to 143.98°C for 2.5 wt % GO loading. The recording of DSC scan also enabled us to observe crystallization temperature during cooling cycle. From Figure 9, it can be seen that the crystallization temperature has decreased from 127.59°C for 0.5 wt % GO loading to 130.86°C for 3 wt % GO loading. These results indicate that the incorporation of GO in PEDOT-block-PEG/PVDF matrix made the nanocomposites thermally more stable. The thermal stability of PEDOT-block-PEG/PVDF/GO nanocomposites was evaluated by TGA. Figure 10 shows the TGA curves of PEDOT-block-PEG/PVDF/GO nanocomposites. The initial mass reduction at 200°C is due to

labile oxygen containing functional groups, resulting in a rapid thermal expansion of the material. During this degradation process, most of the oxygen containing functional groups of GO are removed. The second weight loss in the temperature range 480-500^{o}C occurred due to decomposition of PVDF and PEDOT-block-PEG from the nanocomposites. So there is a significant rise in thermal stability of nanocomposites. These results suggest that GO acts as an effective barrier due to its large aspect ratio which prevented the emission of small gas molecules during thermal degradation.[40]

Surface morphology and surface roughness

AFM characterization has been one of the most direct methods of quantifying the degree of exfoliation in dispersion of GO powder and a solvent. The surface microstructure and roughness of the composite films were characterized by using AFM in a tapping mode and the results are depicted in Figure 11 - Figure 13. It was observed that GO as filler has a significant effect over the surface morphology of nanocomposite films. The surface of nanocomposites was found to be non uniform which may be due to increase in GO loading. The average surface roughness observed for 0.5 wt% GO loading was 34.37±0.01 nm which increases up to 787.98±0.02 nm for 2.5 wt% GO loading. Surface roughness of the PEDOT-block-PEG/PVDF/GO nanocomposite films increases drastically upon loading of the GO in PEDOT-block-PEG matrix. This may be due to full exfoliation and fine dispersion of GO throughout the PEDOT-block-PEG/PVDF matrix. Surface roughness has an enormous influence on many important physical properties such as wettability, adhesion, friction etc. Surface roughness can also be useful for the formation of coating on superhydrophobic surfaces. The increase in surface roughness of polymer nanocomposites is attractive because rough surface brings strong mechanical interlocking between the nanofiller and polymer matrix leading to increase in the properties of nanocomposite.[41] Hence the AFM data supports that the surface roughness can be tuned by controlled incorporation of GO within the polymer matrix. The homogeneous dispersion of PEDOT-block-PEG/PVDF/GO in DMF can be achieved for the successful preparation of nanocomposites.

Dielectric Properties of PEDOT-block-PEG/PVDF/GO nanocomposites

Figure 14 (a-f) shows the plots of dielectric constant of PEDOT-block-PEG/PVDF/GO nanocomposites films in the frequency range 50 Hz to 35 MHz and temperature in the range 40-150^{o}C. All nanocomposites show significant improvement in dielectric constant at lower frequency and with further increase in frequency the dielectric constant values decreases. A comparative data of dielectric constant and dielectric loss of PEDOT-block-PEG/PVDF/GO nanocomposites is given in Table 2, where, it can be seen that, the dielectric constant values increases from 58.684 at 50 Hz and at 130^{o}C for 0.5 wt % GO loading to 266.091 at 50 Hz and at 100^{o}C for 3 wt % GO loading. The increment in dielectric constant values for nanocomposites at lower frequency is because at lower frequency region the alternation of field is slow which provides sufficient time to permanent and induced dipoles to align themselves according to applied electric field. This leads to enhanced polarization. The enhanced dielectric constant values at lower frequency region can be attributed to interfacial polarization and/or electrode polarization because interfacial polarization operates at lower frequencies and it is always present in polymer nanocomposites due to presence of fillers and additives.[42, 43] It is worth mentioning that high aspect ratio fillers such as GO can efficiently increase the dielectric constant of polymer nanocomposites. There are several reports where high dielectric constant has been reported. Srivastava, et. al., reported dielectric constant as high as 7.87x 10^4 at a volume fraction of 0.031 (~ 6 wt %) of foliated graphite.[44] It was reported that styrene-acrylonitrile/graphite sheets (GS) composites exhibits a dielectric constant value of 7.84 x 10^5 at 6 wt % of graphite sheets. Similarly, polystyrene/graphite nanocomposites exhibit a dielectric constant value of 136 at a graphite loading of 6.5 wt %. These composites were recommended for embedded capacitor applications. [45, 46] Furthermore, polyimide/GO nanocomposites exhibit a dielectric constant value as high as 20000 for 5 wt% GO loading.[47] In the present investigation we achieved a dielectric constant value of 266.091 for 3 wt % GO loading.

Figure 15 (a-f) shows the plots of dielectric loss (tanδ) of PEDOT-block-PEG/PVDF/GO nanocomposites in the frequency range of 50 Hz to 35 MHz and the temperature in the range 40-150^{o}C. Dielectric loss increases from 1.758 at 50Hz and at 80^{o}C for 0.5 wt % GO loading to 17.694 at 50 Hz at 30^{o}C for 3 wt % GO loading. As compared to dielectric constant values of all nanocomposites, the dielectric loss values are much lower which is highly attractive for practical

applications such as embedded capacitors. The enhancement in the dielectric properties indicate that the dispersion of GO in PEDOT-block-PEG/PVDF matrix was homogeneous. The π-conjugation in GO layers was interrupts by the presence of functional groups on the surface of GO, and favors the compatibility between the polymer and the filler.[48] Thus, PEDOT-block-PEG/PVDF/GO nanocomposites exhibit a high dielectric constant and relatively low dielectric loss. Hence, the nanocomposites can be recommended for embedded capacitor applications. However, scaling of the polarization mechanism in these nanocomposites as a function of GO loading can produce enhanced dielectric properties, suitable for supercapacitor application which is our interest and further scope of this investigation.

Conclusions

PEDOT-block-PEG/PVDF/GO novel nanocomposites were successfully prepared by colloidal blending and their performance was evaluated using different analytical techniques. FTIR and XRD spectra revealed the successful incorporation of GO into the PEDOT-block-PEG/PVDF matrix. A significant improvement in the thermal stability of the composite was observed which indicates strong interfacial interaction between PEDOT-block-PEG, PVDF and GO. Dielectric properties demonstrated very high dielectric constant and relatively low dielectric loss for PEDOT-block-PEG/PVDF/GO nanocomposites. Better dispersion resulted in an increase in the dielectric constant from 58.684 for 0.5 wt% to 266.091 for 3 wt% GO loading and dielectric loss from 1.758 for 0.5 wt % GO to 17.694 for 3 wt % GO Thus, based on the dielectric results, we conclude that PEDOT-block-PEG/PVDF/GO nanocomposites can be used for embedded capacitor applications.

Acknowledgements

We greatly acknowledge the financial support of Naval Research Board, Defense Research and Development Organization (NRB-DRDO), New Delhi, to carry out this research work under **Project No.259/Mat. /11-12**. Authors also wish to thank Dr. A.B. Samui and Dr. Debdutta Ratna from Naval Materials Research Laboratory (NMRL), Ambernath, Mumbai, India for his insightful comments and valuable suggestions during this research work.

References:

1. C. Soldano, A. Mahmood, E. Dujardin, Carbon 48 (2010) 2127-2150.
2. K. S. Novoselov, A.K. Geim, S.V. Morozov, D. Jian, Y. Zhang, S.V. Dubones, I.V. Grigorieva, A. A. Firsov, Science 306 (2004) 666-669.
3. A. A. Balandin, S. Ghosh, W. Bao, J. Calizo, D. Teweldebrhan, F. Miao, L.C. Ning, Nano Lett 8 (2008) 902-907.
4. C. Lee, X. Wei, J.W.Kysar, J. Hone, Science 321 (2008) 385-388.
5. T. Kuilla, S. Bhadra, D. Yao, N.H. Kim, S. Bose, J.H. Lee, Prog Polym Sci 35 (2010) 1350-1375.
6. F. Schedin, A.K. Geim, S.V. Morozov, E. W. Hill, P. Blake, M.I. Kats-nelson, K. S. Novoselov, Nat Mater 6 (2007) 652-655.
7. M. D. Stoller, S. Park, Y. Zhu, J. An, R.S. Ruoff, Nano Lett 8 (2008)3498-3502.
8. X. Wang, L. Zhi, K. Mullen, Nano Lett 8 (2008) 323-327.
9. X. Wang, X. Li, L. Zhang, Y. Yoon, P.K. Weber, H. Wang, J. Guo, H. Dia, Science, 324 (2009) 768-771.
10. E. Yoo, J. Kim, E. Hosono, H. Zhou, T. Kudo, I. Honma, Nano Lett 8 (2008) 2277-2282.
11. A. Reina, X.T. Jia, J. Ho, D. Nezich, H.B. Son, V. Bulovic, M.S. Dresselhaus, J. Kong, Nano Lett, 9 (2009) 30-35.
12. C. Berger, Z.M.Song, X.B. Li, X. S. Wu, N. Brown, C. Naud, D. Mayou, T. Li, J. Hass, A. N. Marchenkov, E. H. Conrad, P.N. First, W.A.de Heer, Science 312(2006)1191-1196.
13. D. A. Dikin, S. Stankovich, E.J. Zimmey, R. D. Piner, G. H. B. Dommett, G. Evmeneko, S. T. Nguyen, R.S. Ruoff, Nature 448 (2007) 457-460.
14. K. Krishnamoorthy, M. Veerapandian, K. Yun, S.J. Kim, Carbon, 53 (2013)38-49.
15. D.R. Daniel, P. Sungjin, W. B. Christopher, R.S. Ruoff, Chem Soc Rev 39 (2010) 228-240.
16. K.N. Kudin, B. Ozbas, H. C. Schniepp, R. K. Prudhomme, A. A. Aksay, R. Car, Nano Lett 8 (2007) 36-41.
17. G. Wang, X. Sun, C. Li, J. Lian, Appl Phys Lett 99 (2011) 053114.
18. K. Krishnamoorthy, R. Mohan, S. J. Kim, Appl Phys Lett 98(2011)1-3.
19. Q. Chang, J. Tang, J. Ma, H. Zhang, N. Shinya, L. C. Qin, Carbon 49(2011)2917-2925.

20. K. Deshmukh, G. M. Joshi, Polymer Testing, 34(2014) 211-219.
21. H. Tai, Y. Jiang, G. Xie, J. Yu, J Mater Sci 26 (2010) 605-613.
22. C. Basavaraja, W.J. Kim, Y. D. Kim, D. S. Huh, Mater Lett 65(2011)3120-3123.
23. X. Wang, Y.G. Kim, C. Drew, B. C. Ku, J. Kumar, L. A. Samuelsen, Nano Lett 4 (2004) 331-334.
24. K. Y. Chao, H. G. Lim, S. R. Yun, J. Kim. K.S. Kang, J Phys Chem C112 (2008)7001-7004.
25. H. Wang, Q. Hao, X. Yang, L. Lu, X. Wang, Nanoscale 2 (2010) 2164-2170.
26. N. Perinka, C. H. Kim, M. Kaplanova, Y. Bonnassieux, Phys Procedia 44(2013) 120-129.
27. L. Groenendal, J. Dhaen, J. Manca, J. Vanluppen, E. Verdonk, F. Louwet, L. Leenders, Synthetic Metals,135-136(2003)115-117.
28. W.S. Hummers, R.E. Offman, J Amer Chem Soc 80 (1958) 1339-1339.
29. K. Deshmukh, S. M. Khatake, G.M. Joshi, J Polym Res 20 (2013) 286.
30. Y. Xu, Y. Wang, J. Liang, Y. Huang, Y. Ma, X. Wan, Y. Chen, Nano Res 2 (2009) 343-348.
31. Y. A. Udum, K. Pekmez, A. Yildiz, Eur Polym J, 40(2004) 1057-1062.
32. S. M. Pawde, K. Deshmukh, J Appl Polym Sci 114 (2009) 2169-2179.
33. S. M. Pawde, K. Deshmukh, J Appl Polym Sci 101 (2006) 4167-4171.
34. S. M. Pawde, K. Deshmukh, Polym Eng Sci 49 (2009) 808-818.
35. Z. Ni, Y. Wang, T.Yu, Z. Shen, Nano Res, 1(2008) 273-291.
36. Y. Guo, B. Chenlu, L. Song, B.Yuan, Y. Hu, Ind Eng Chem Res 50 (2011) 7772-7783.
37. J. R. Dryer, Application of Absorption Spectroscopy of Organic Compounds, Prentice Hall Inc., NJ, USA (1994).
38. J. Wu, Appl Surf Sci, 257 (2010)747-751.
39. R. Koizhaiganova, H.J.Kim, T.Vasudevan, S.Kudaibergenov, M.S. Lee, J Appl Polym Sci, 115 (2010) 2448-2454.
40. T. Kuila, S. Bose, A. K. Mishra, P. Khanra, N. H. Kim, J. H. Lee, Polymer Testing, 31(2012) 31-38.
41. J. Wang, P. Chen, C. Luo, H. Chen, H. Chen, H. Li, B.L.Sun, Surf Coat Tech 203 (2009) 3722-3727.
42. D. Wang, T. Zhao, J. W.Zha, J. Zhao, Z.M. Dang, J Mater Chem A 1 (2013) 6261-6168.

43. S. Xie, B. Zhu, Z. Xu, Y. Xu, Mater Lett 59 (2005)2403-2407.

44. N.K. Srivastava, R. M. Mehra, J Appl Polym Sci 109 (2008)3991-3999.

45. V. Panwar, R. M. Mehra, Euro Polym J, 44(2008) 2367-2375.

46. M. Xiao, L. Sun, J. Liu, Y. Li, K. Gong, Polymer 43(2002)2245-2248.

47. J. Y. Kong, M. C. Choi, G. Y. Kim, J. J. Park, M. Selvaraj, M. Han, C.S. Ha, Euro Polym J 48(2012)1394-1405.

48. R.R. Kohlmeyer, A. Jawadi, B. Pradhan, S. Pilla, K. Setyowati, J. Chen, S.Q. Gong, J Phys Chem C 113 (2009) 17626-17629.

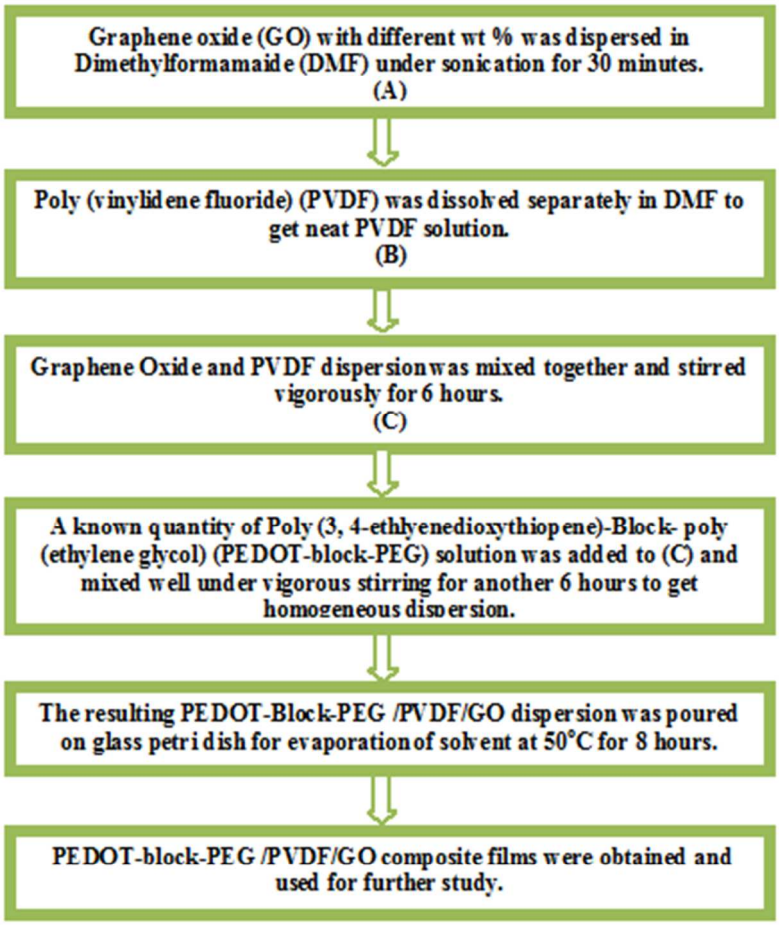

Figure 1: Protocol for synthesis of PEDOT-block-PEG/PVDF/GO pristine nanocomposites

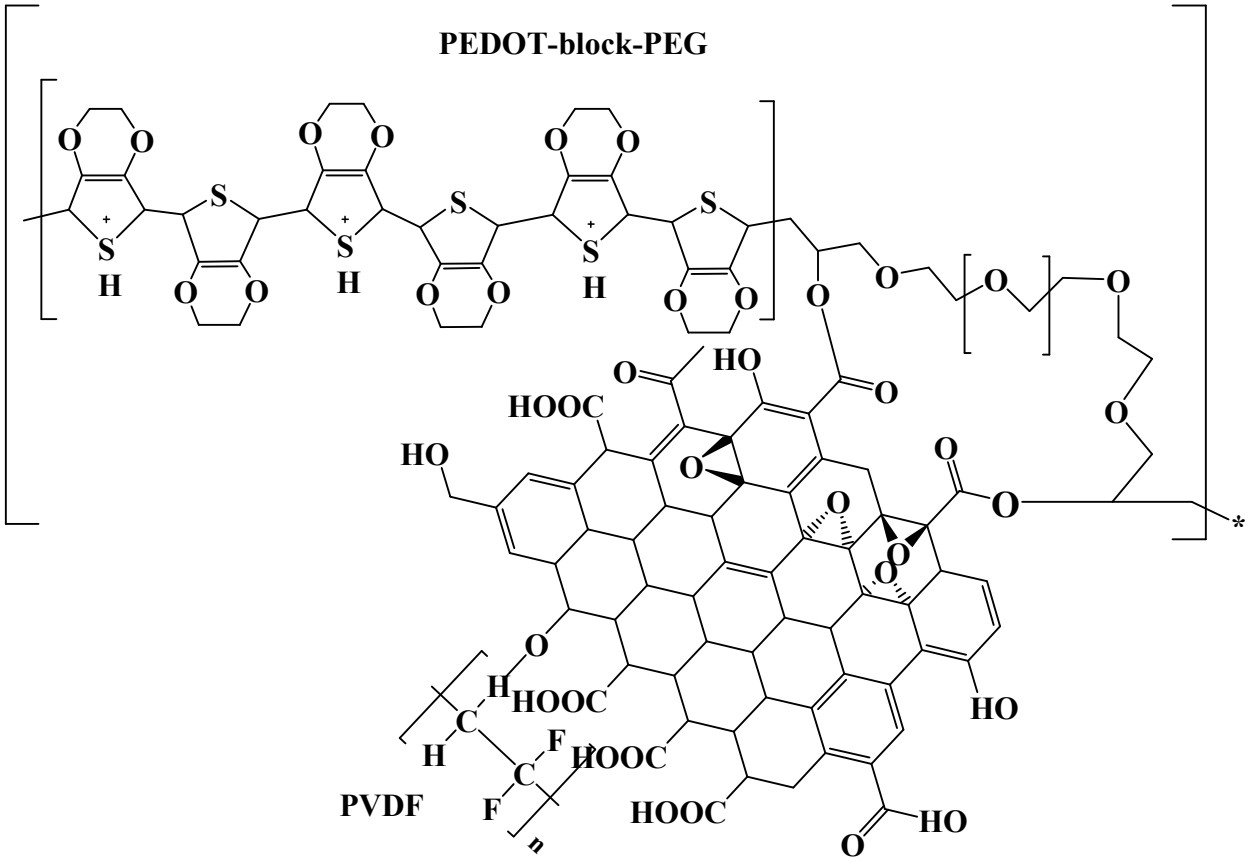

Figure 2: Schematic representation of the bonding interaction between PEDOT-block-PEG, PVDF and GO.

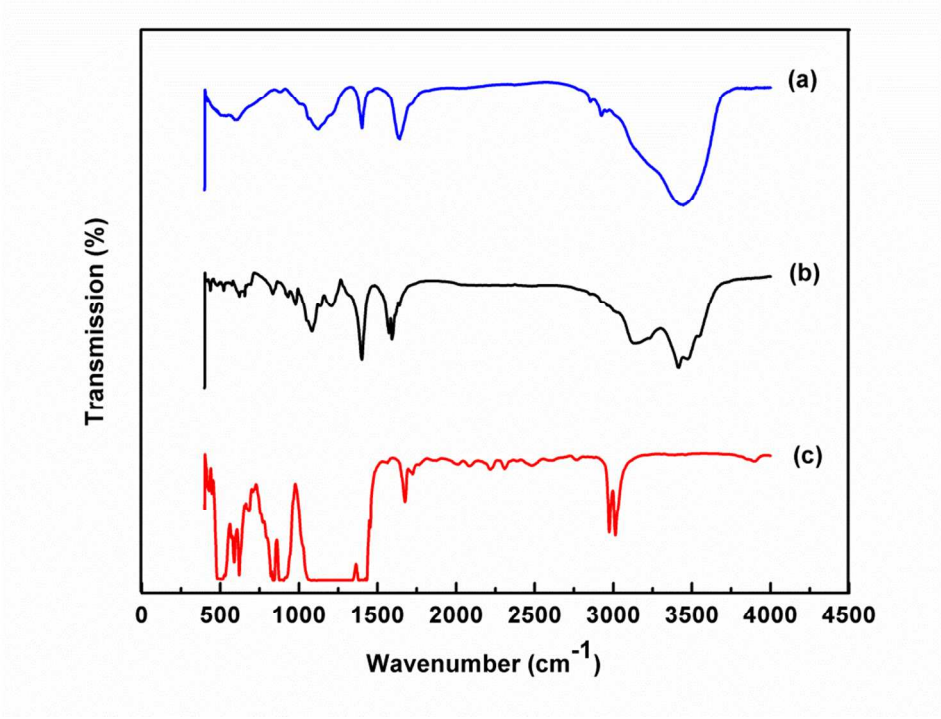

Figure 3: FTIR spectra of (a) GO (b) Pure PEDOT-block-PEG (c) Pure PVDF.

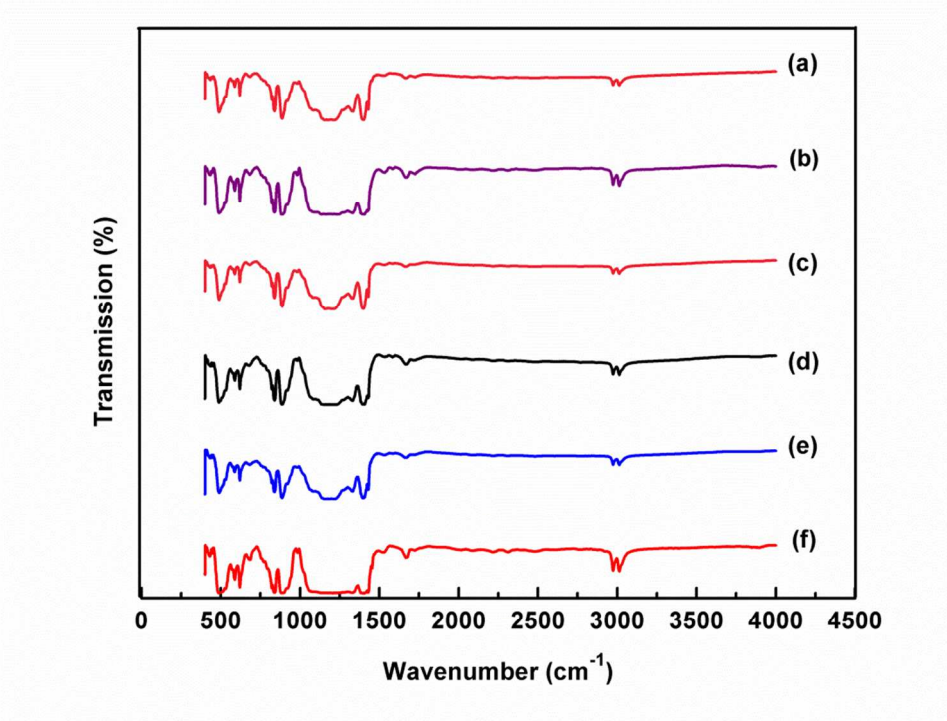

Figure 4: FTIR spectra of PEDOT-block-PEG/PVDF/GO nanocomposite film (a) 0.5 wt% GO (b) 1wt% GO (c) 1.5wt% GO (d) 2 wt% GO (e) 2.5 wt% GO (f) 3 wt% GO.

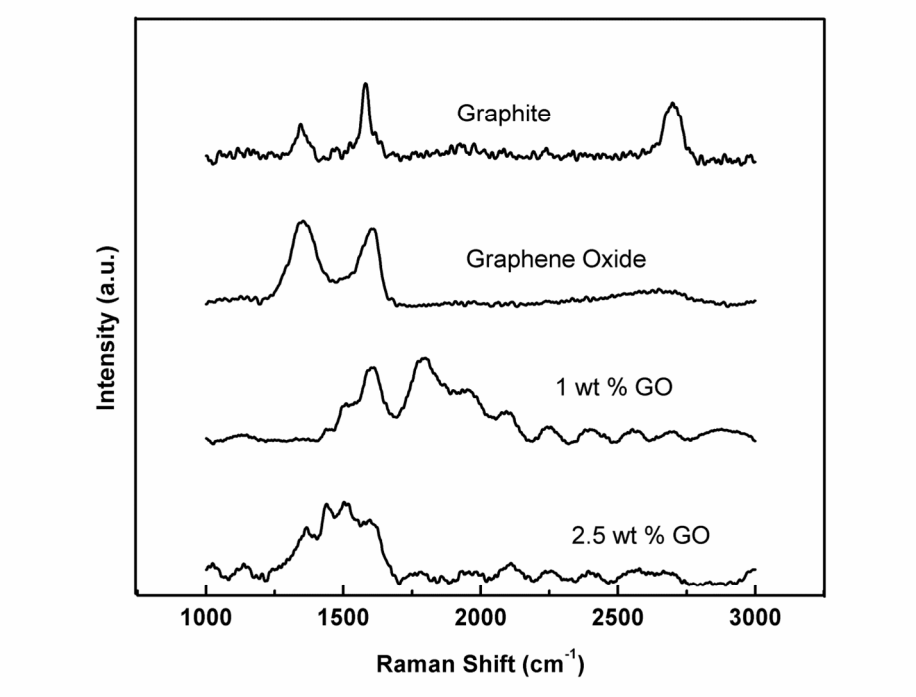

Figure 5: Raman Spectra of graphite GO and PEDOT-block-PEG/PVDF/GO nanocomposites with 1 and 2.5 wt % GO.

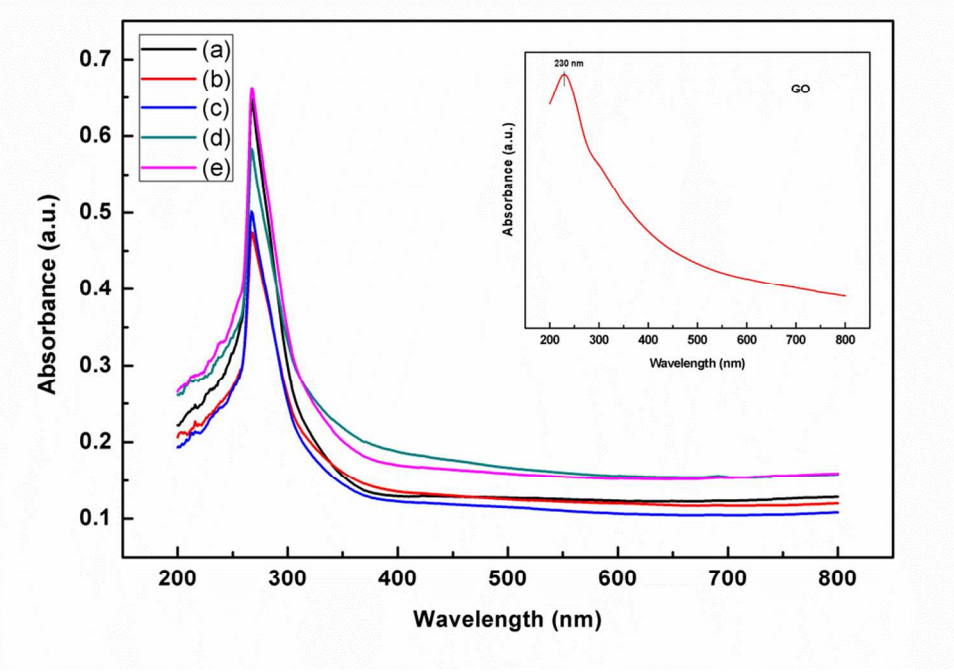

Figure 6: UV-vis spectra of PEDOT-block-PEG/PVDF/GO nanocomposites (a) 0.5 wt% GO (b) 1wt% GO (c) 1.5wt% GO (d) 2wt% GO (e) 2.5 wt% GO (Inset: UV-vis spectrum of GO).

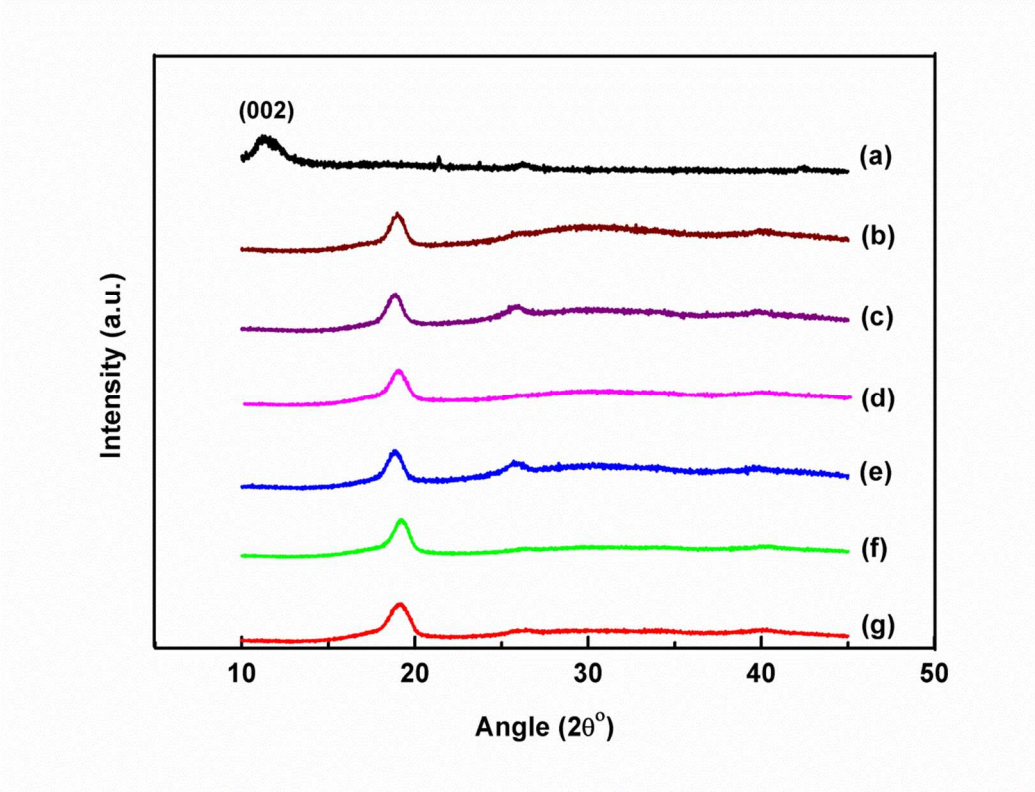

Figure 7: XRD spectra of PEDOT-block-PEG/PVDF/GO composites (a) GO (b) 0.5 wt% GO (c) 1 wt% GO (d) 1.5 wt% GO (e) 2 wt% GO (f) 2.5 wt% GO.

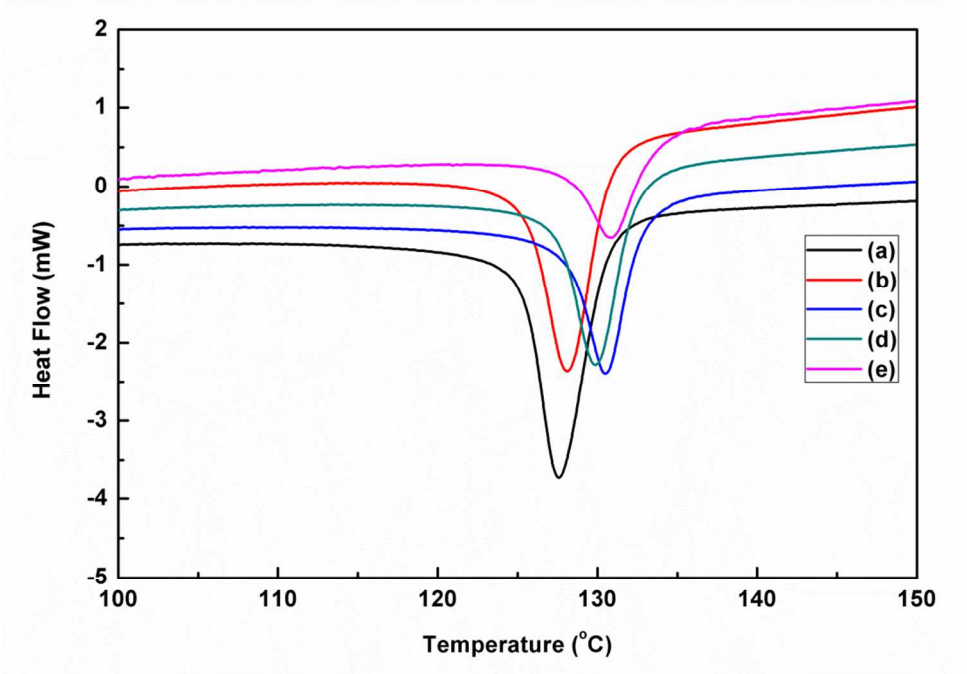

Figure 8: DSC melting thermograms of PEDOT-block-PEG/PVDF/GO composites (a) 0.5 wt% GO (b) 1 wt% GO (c) 1.5 wt% GO (d) 2 wt% GO (e) 2.5 wt% GO.

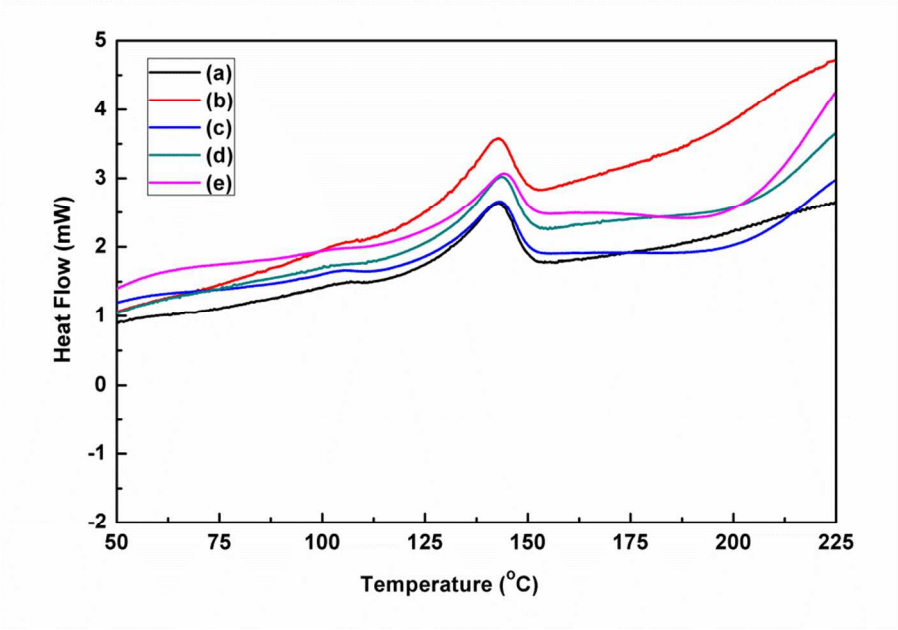

Figure 9: Crystallization temperature of PEDOT-block-PEG/PVDF/GO composites (a) 0.5 wt% GO (b) 1 wt% GO (c) 1.5 wt% GO (d) 2 wt% GO (e) 2.5 wt% GO.

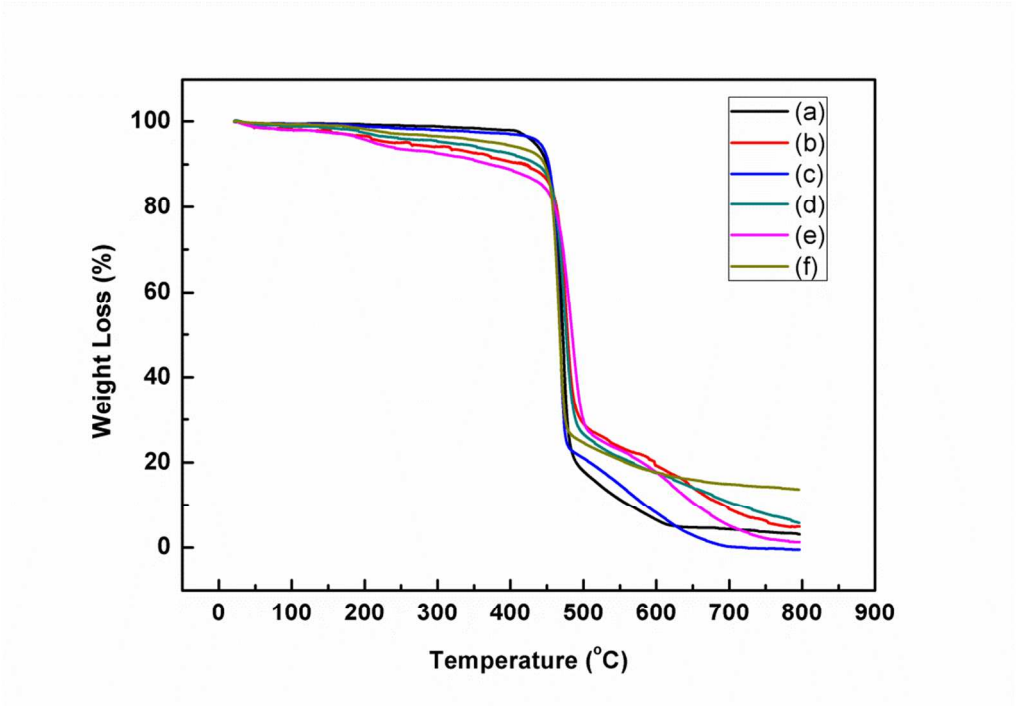

Figure 10: Weight Loss as a function of temperature for different PEDOT-block-PEG/PVDF/GO composites (a) 0.5 wt% GO (b) 1 wt% GO (c) 1.5 wt% GO (d) 2 wt% GO (e) 2.5 wt% GO (f) 3 wt% GO.

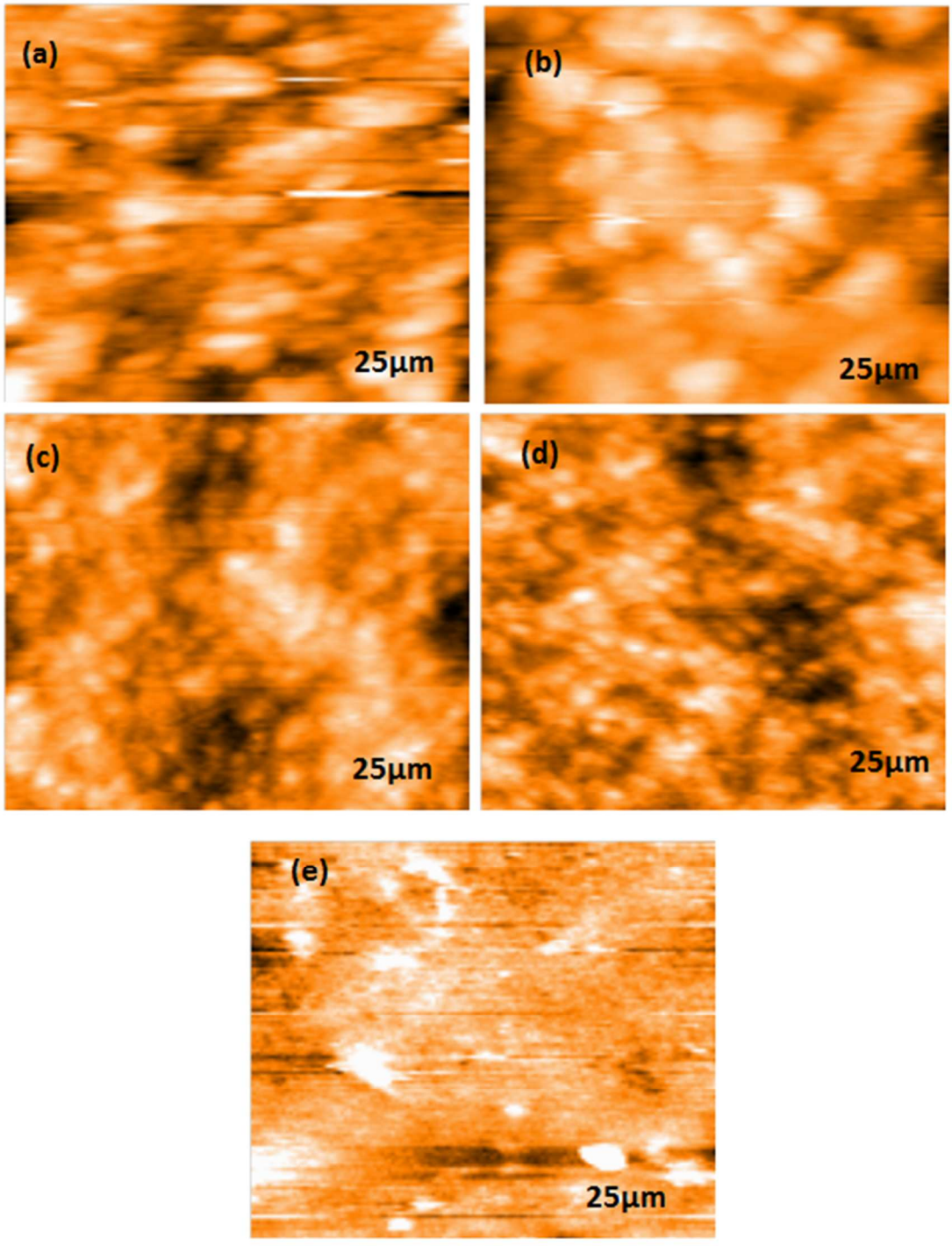

Figure 11: AFM topographic images of PEDOT-block-PEG/PVDF/GO composites (a) 0.5wt% GO (b) 1 wt% GO (c) 1.5 wt% GO (d) 2 wt% GO (e) 2.5 wt% GO

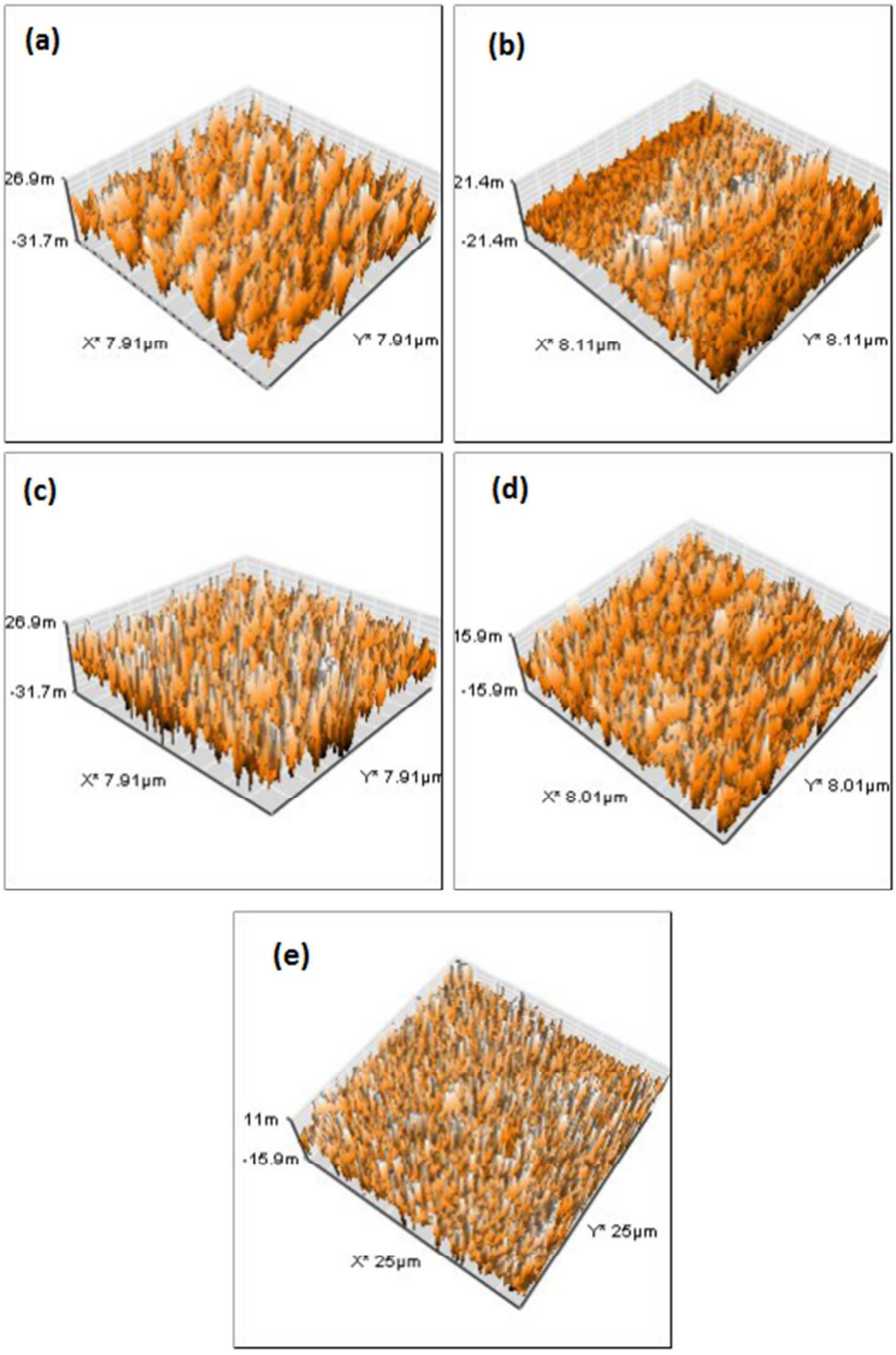

Figure 12: AFM 3D images of PEDOT-block-PEG/PVDF/GO composites (a) 0.5wt% GO (b) 1 wt% GO (c) 1.5 wt% GO (d) 2 wt% GO (e) 2.5 wt% GO

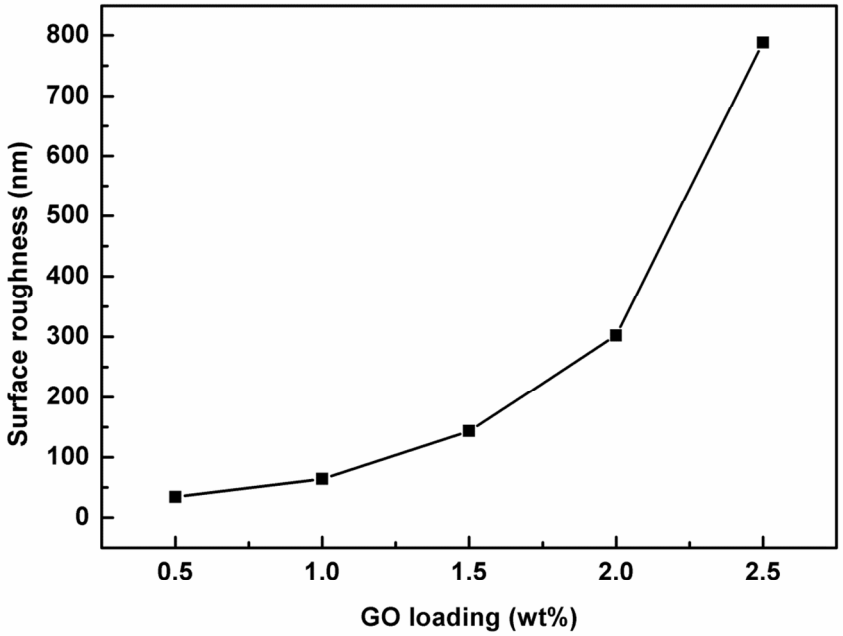

Figure 13: Variation in surface roughness of PEDOT-block-PEG/PVDF/GO composites as a function of GO loading.

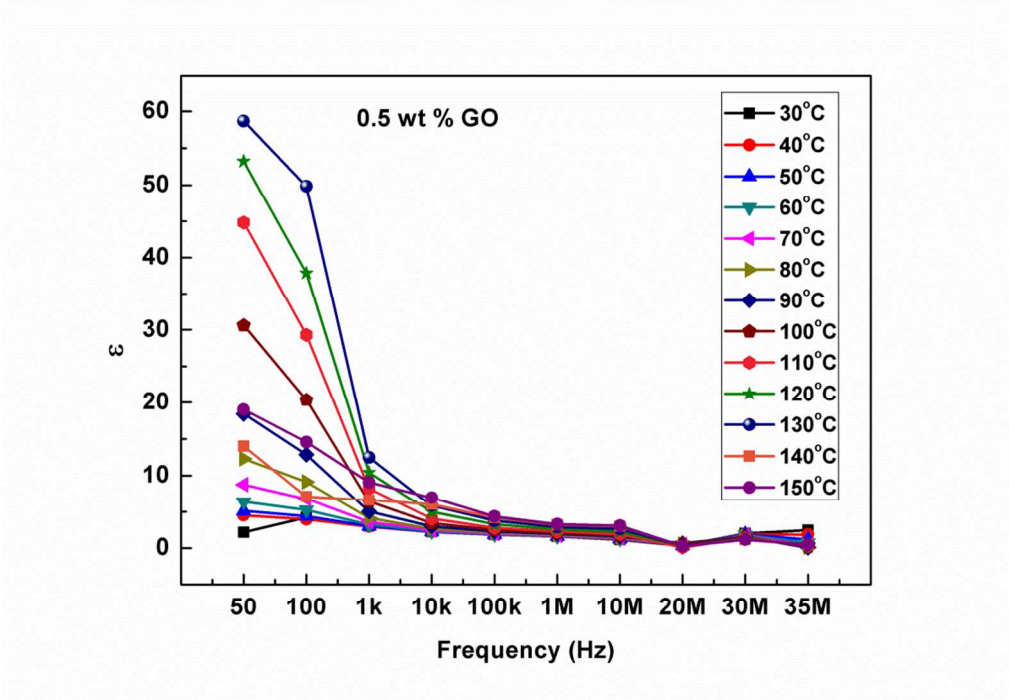

Figure 14 (a): Variation in dielectric constant of PEDOT-block-PEG/PVDF/GO nanocomposites with 0.5 wt% GO loading as a function of frequency at various temperatures.

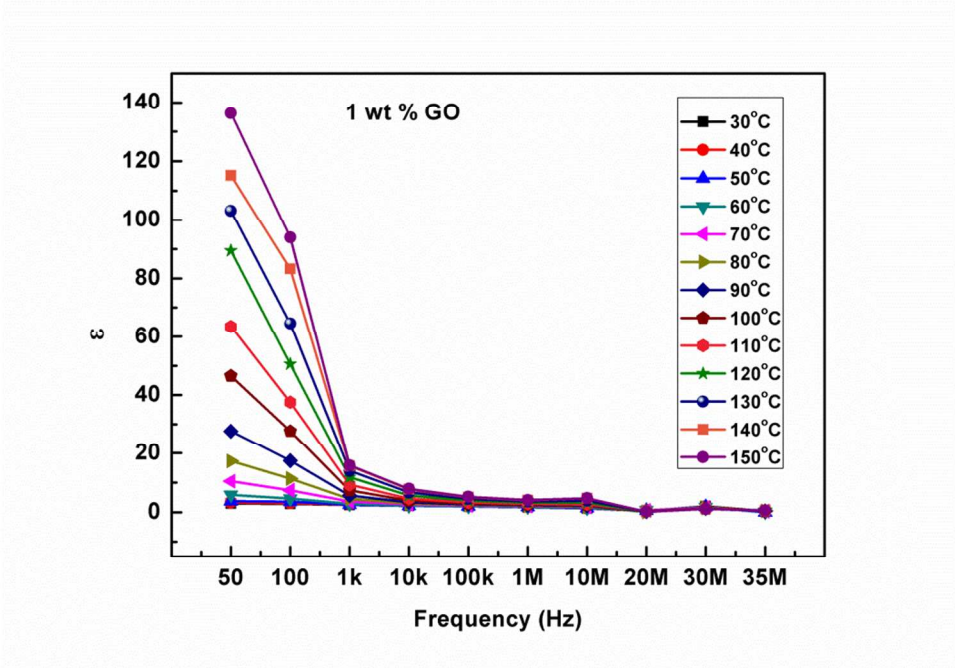

Figure 14 (b): Variation in dielectric constants of PEDOT-block-PEG/PVDF/GO nanocomposite with 1 wt% GO loading as a function of frequency at various temperatures.

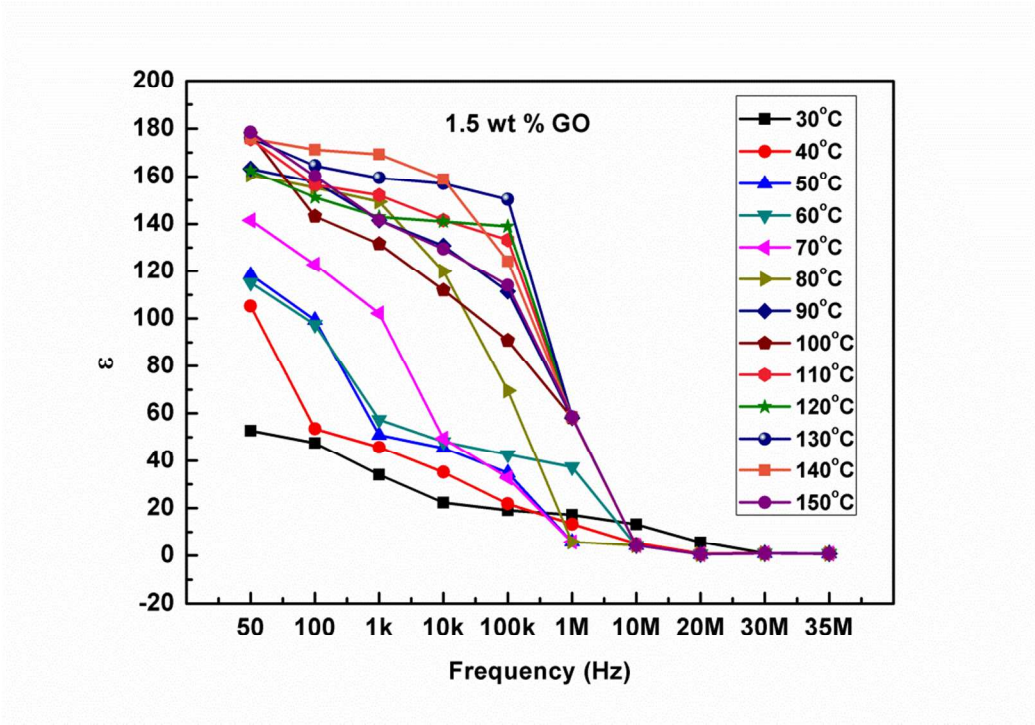

Figure 14 (c): Variation in dielectric constants of PEDOT-block-PEG/PVDF/GO nanocomposite with 1.5 wt% GO loading as a function of frequency at various temperatures.

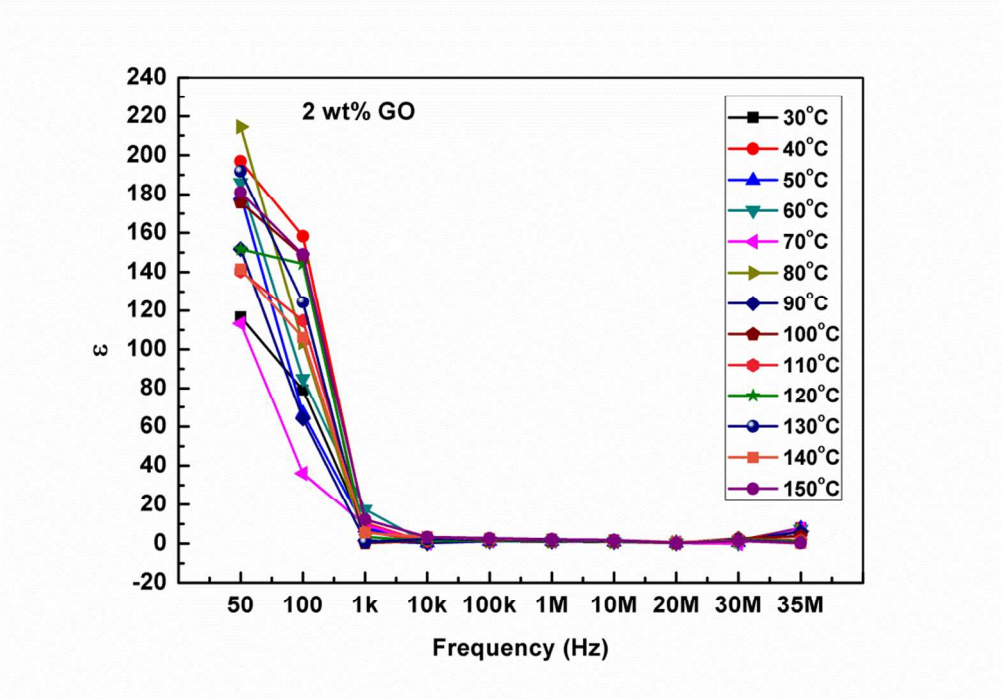

Figure 14 (d): Variation in dielectric constants of PEDOT-block-PEG/PVDF/GO nanocomposite with 2 wt% GO loading as a function of frequency at various temperatures.

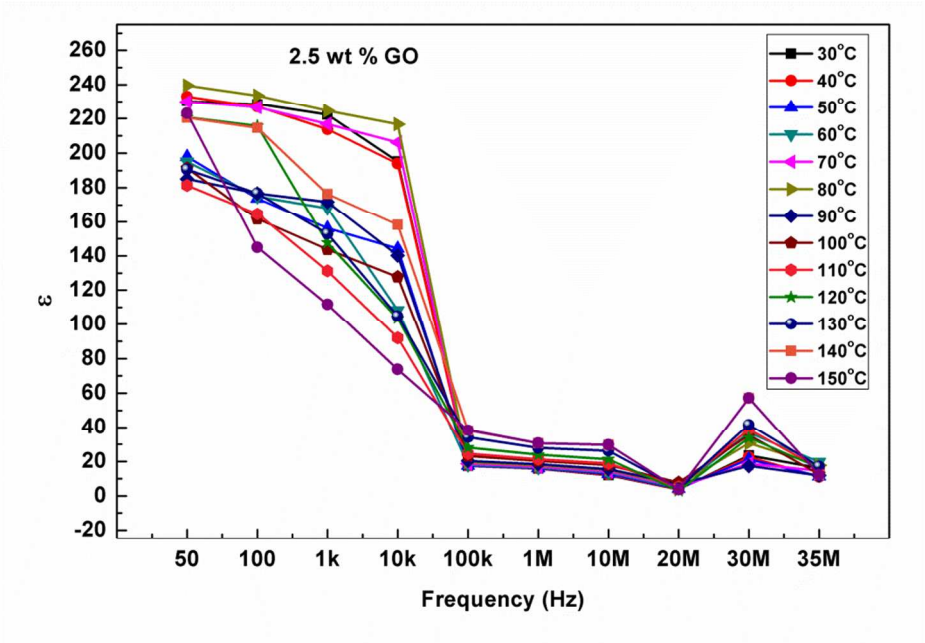

Figure 14 (e): Variation in dielectric constants of PEDOT-block-PEG/PVDF/GO nanocomposite with 2.5 wt% GO loading as a function of frequency at various temperatures.

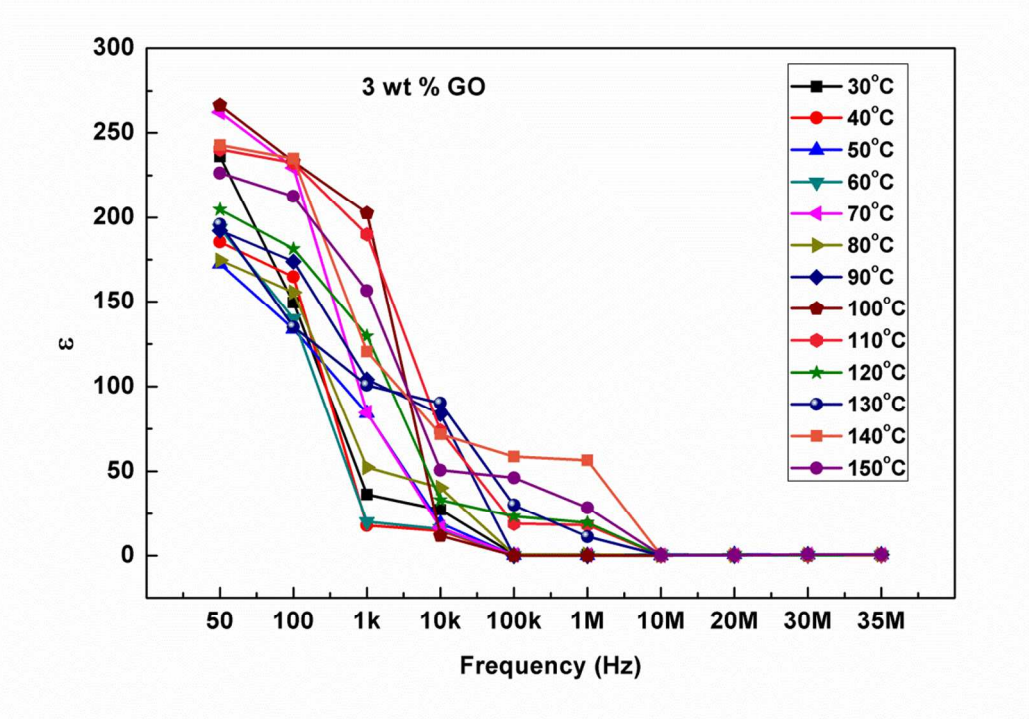

Figure 14 (f): Variation in dielectric constants of PEDOT-block-PEG/PVDF/GO nanocomposite with 3 wt% GO loading as a function of frequency at various temperatures.

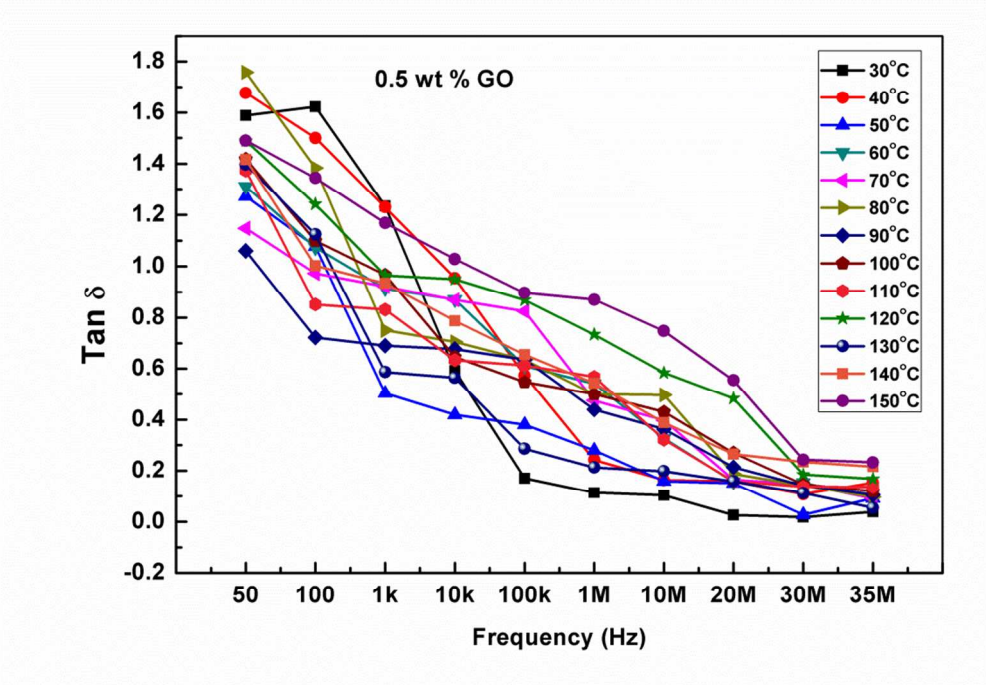

Figure 15 (a): Variation in dielectric loss of PEDOT-block-PEG/PVDF/GO nanocomposites with 0.5 wt% GO loading as a function of frequency at various temperatures.

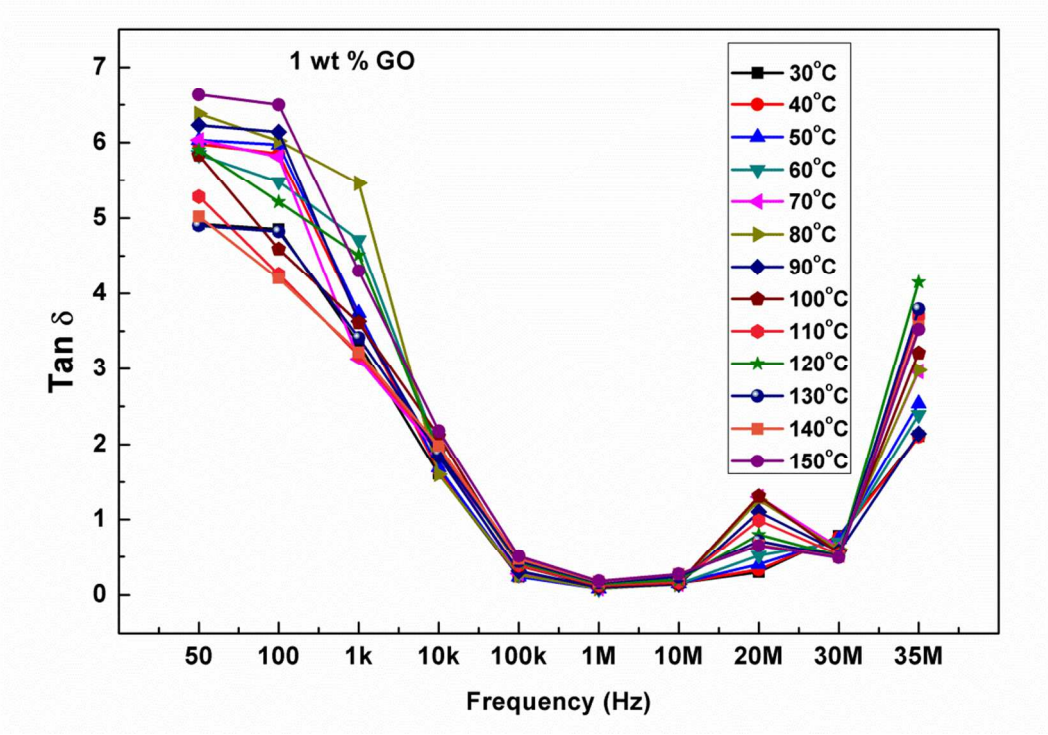

Figure 15 (b): Variation in dielectric loss of PEDOT-block-PEG/PVDF/GO nanocomposite with 1wt% GO loading as a function of frequency at various temperatures.

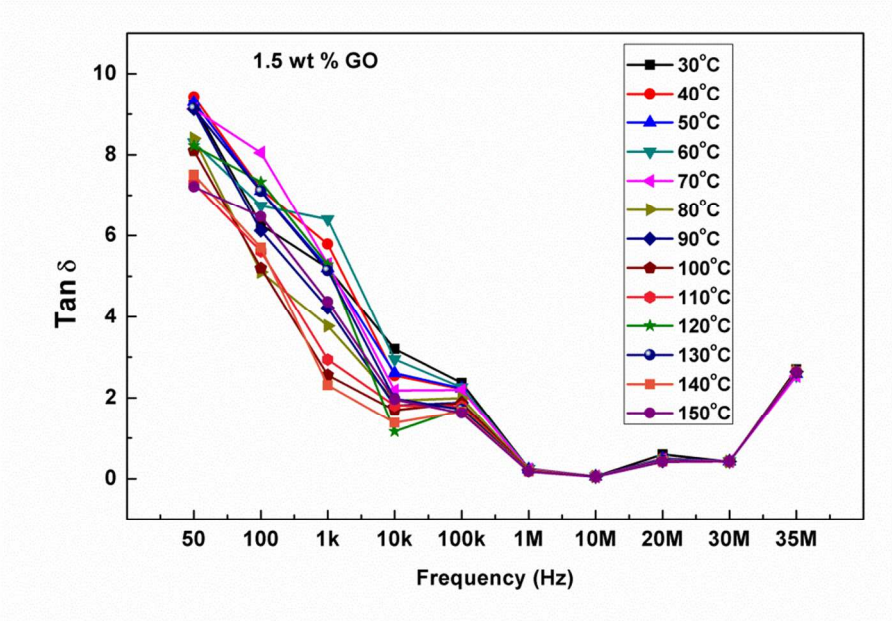

Figure 15 (c): Variation in dielectric loss of PEDOT-block-PEG/PVDF/GO nanocomposite with 1.5wt% GO loading as a function of frequency at various temperatures.

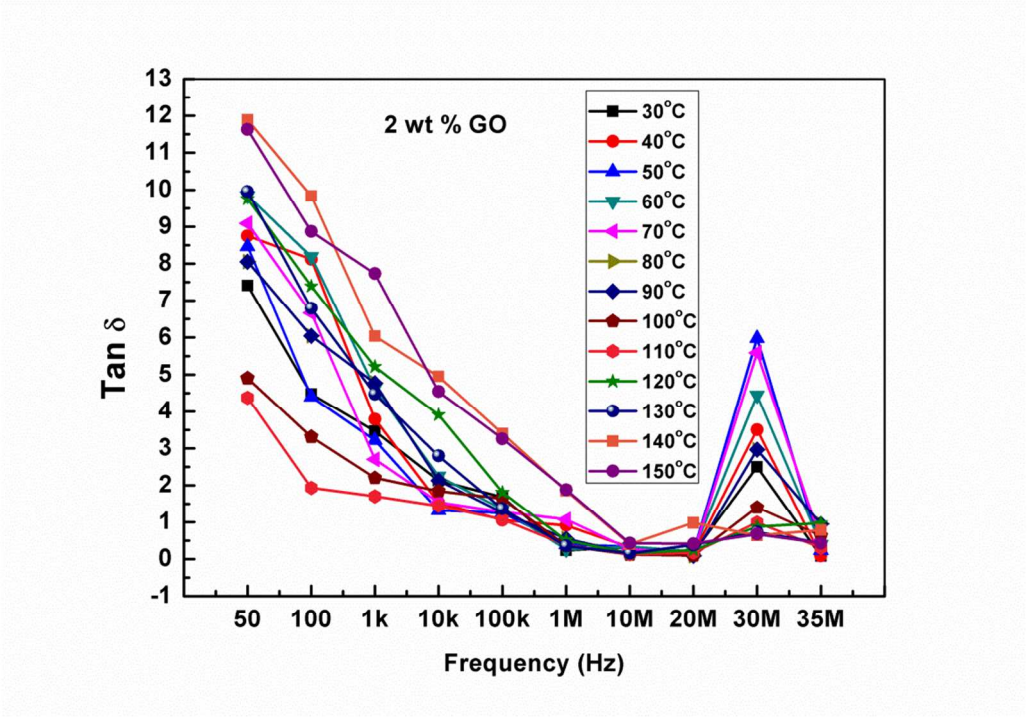

Figure 15 (d): Variation in dielectric loss of PEDOT-block-PEG/PVDF/GO nanocomposite with 2 wt% GO loading as a function of frequency at various temperatures.

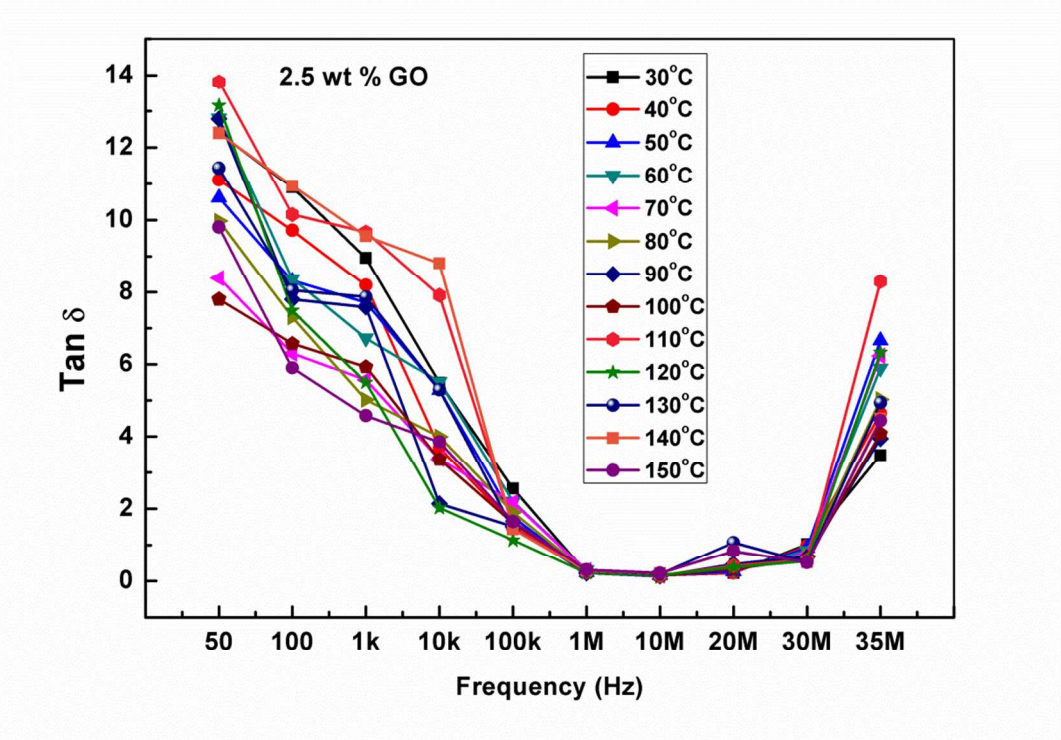

Figure 15 (e): Variation in dielectric loss of PEDOT-block-PEG/PVDF/GO nanocomposite with 2.5wt% GO loading as a function of frequency at various temperatures.

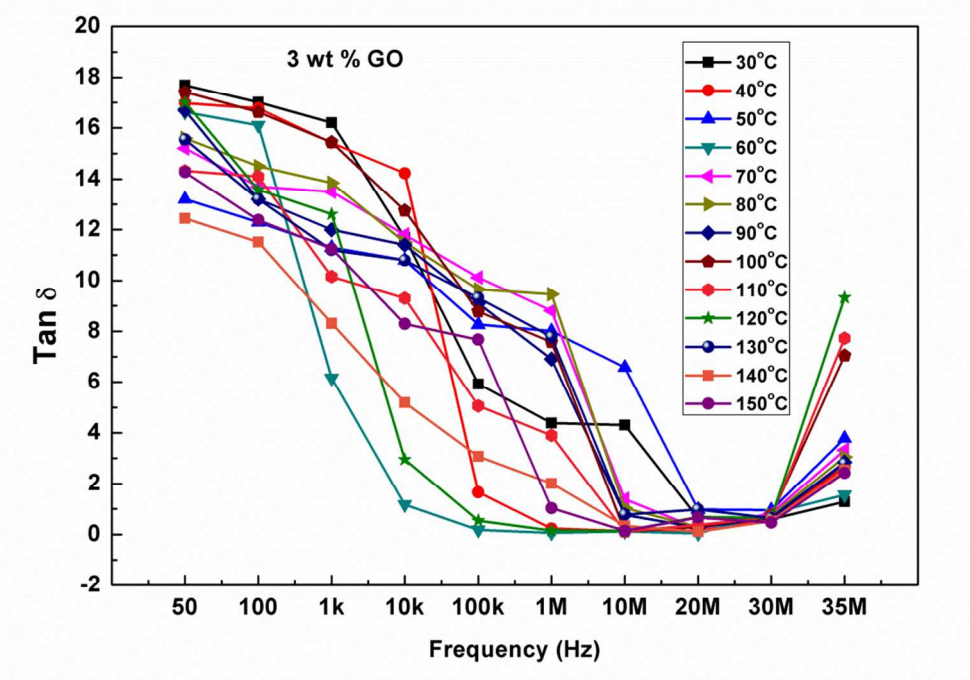

Figure 15 (f): Variation in dielectric loss of PEDOT-block-PEG/PVDF/GO nanocomposite with 3 wt% GO loading as a function of frequency at various temperatures.

Table 1: FTIR peak assignments for GO, PVDF and PEDOT-block-PEG.

FTIR Peak assignments for GO		**FTIR Peak assignments for PVDF**		**FTIR Peak Assignments for PEDOT-block-PEG**	
Wavenumbers (cm^{-1})	**Assignments**	**Wavenumbers (cm^{-1})**	**Assignments**	**Wavenumbers (cm^{-1})**	**Assignments**
3419	O-H Stretching	3012	Asymmetric stretching vibration of CH_2 group	2933	C-H Stretching
1720	C=O Stretching	2974	Symmetric stretching vibration of CH_2 group	1571	C=C Stretching
1643	C=C Stretching	1064	CF_2 Stretching vibrations	1400	C=C Stretching
1404	C-O Stretching	842	CH_2 Rocking vibrations	1083	C-H Bending
1124	C-O Stretching	588	CF_2 bending vibrations	979	C-S Bond
				835	C-S Bond
				623	C-S Bond

Table 2: Comparative values of dielectric constant and dielectric loss of nanocomposites as a function of GO loading.

GO Loading (wt %)	**Dielectric Constant (ε)**	**Dielectric Loss (Tan δ)**
0.5	58.684, 50 Hz, 130°C	1.758, 50Hz, 80°C
1	136.302, 50 Hz, 150°C	6.634, 50Hz, 150°C
1.5	178.443, 50 Hz, 150°C	9.428,50 Hz, 40°C
2	214.418, 50 Hz, 80°C	11.891, 50Hz, 140°C
2.5	239.538, 50 Hz, 80°C	13.813, 50Hz, 110°C
3	266.091, 50Hz, 100°C	17.694, 50 Hz, 30°C

Figure and Table Captions:

Figure 1: Protocol for synthesis of PEDOT-block-PEG/PVDF/GO pristine nanocomposites.

Figure 2: Schematic representation of the bonding interaction between PEDOT-block-PEG, PVDF and GO.

Figure 3: FTIR spectra of (a) GO (b) Pure PEDOT-block-PEG (c) Pure PVDF.

Figure 4: FTIR spectra of PEDOT-block-PEG/PVDF/GO nanocomposite film (a) 0.5 wt% GO (b) 1wt% GO (c) 1.5wt% GO (d) 2 wt% GO (e) 2.5 wt% GO (f) 3 wt% GO.

Figure 5: Raman Spectra of Graphite, GO and PEDOT-block-PEG/PVDF/GO nanocomposite with 1 wt % GO and 2.5 wt % GO.

Figure 6: UV-vis spectra of PEDOT-block-PEG/PVDF/GO composites (a) 0.5 wt% GO (c) 1wt% GO (d) 1.5wt% GO (e) 2wt% GO (f) 2.5 wt% GO

Figure 7: XRD spectra of PEDOT-block-PEG/PVDF/GO composites (a) 0.5 wt% GO (b) 1 wt% GO (c) 1.5 wt% GO (d) 2 wt% GO (e) 2.5 wt% GO (f) 3 wt% GO.

Figure 8: DSC melting thermograms of PEDOT-block-PEG/PVDF/GO composites (a) 0.5 wt% GO (b) 1 wt% GO (c) 1.5 wt% GO (d) 2 wt% GO (e) 2.5 wt% GO.

Figure 9: Crystallization temperature of PEDOT-block-PEG/PVDF/GO composites (a) 0.5 wt% GO (b) 1 wt% GO (c) 1.5 wt% GO (d) 2 wt% GO (e) 2.5 wt% GO.

Figure 10: Weight Loss as a function of temperature for different PEDOT-block-PEG/PVDF/GO composites (a) 0.5 wt% GO (b) 1 wt% GO (c) 1.5 wt% GO (d) 2 wt% GO (e) 2.5 wt% GO (f) 3 wt% GO.

Figure 11: AFM topographic images of PEDOT-block-PEG/PVDF/GO composites (a) 0.5wt% GO (b) 1 wt% GO (c) 1.5 wt% GO (d) 2 wt% GO (e) 2.5 wt% GO

Figure 12: AFM 3D images of PEDOT-block-PEG/PVDF/GO composites (a) 0.5wt% GO (b) 1 wt% GO (c) 1.5 wt% GO (d) 2 wt% GO (e) 2.5 wt% GO (f) 3 wt% GO.

Figure 13: Variation in surface roughness of PEDOT-block-PEG/PVDF/GO composites as a function of GO loading.

Figure 14 (a): Variation in dielectric constant of PEDOT-block-PEG/PVDF/GO nanocomposites with 0.5 wt% GO loading as a function of frequency at various temperatures.

Figure 14 (b): Variation in dielectric constants of PEDOT-block-PEG/PVDF/GO nanocomposite with 1 wt% GO loading as a function of frequency at various

temperatures.

Figure 14 (c): Variation in dielectric constants of PEDOT-block-PEG/PVDF/GO nanocomposite with 1.5 wt% GO loading as a function of frequency at various temperatures.

Figure 14 (d): Variation in dielectric constants of PEDOT-block-PEG/PVDF/GO nanocomposite with 2 wt% GO loading as a function of frequency at various temperatures.

Figure 14 (e): Variation in dielectric constants of PEDOT-block-PEG/PVDF/GO nanocomposite with 2.5 wt% GO loading as a function of frequency at various temperatures.

Figure 14 (f): Variation in dielectric constants of PEDOT-block-PEG/PVDF/GO nanocomposite with 3 wt% GO loading as a function of frequency at various temperatures.

Figure 15 (a): Variation in dielectric loss of PEDOT-block-PEG/PVDF/GO nanocomposites with 0.5 wt% GO loading as a function of frequency at various temperatures.

Figure 15(b): Variation in dielectric loss of PEDOT-block-PEG/PVDF/GO nanocomposite with 1wt% GO loading as a function of frequency at various temperatures.

Figure 15 (c): Variation in dielectric loss of PEDOT-block-PEG/PVDF/GO nanocomposite with 1.5wt% GO loading as a function of frequency at various temperatures.

Figure 15 (d): Variation in dielectric loss of PEDOT-block-PEG/PVDF/GO nanocomposite with 2 wt% GO loading as a function of frequency at various temperatures.

Figure 15 (e): Variation in dielectric loss of PEDOT-block-PEG/PVDF/GO nanocomposite with 2.5wt% GO loading as a function of frequency at various temperatures.

Figure 15 (f): Variation in dielectric loss of PEDOT-block-PEG/PVDF/GO nanocomposite with 3 wt% GO loading as a function of frequency at various temperatures.

Tables:

Table 1: FTIR peak assignments for GO, PVDF and PEDOT-block-PEG.

Table 2: Comparative values of dielectric constant and dielectric loss of nanonanocomposites as a function of GO loading.